Asian Journal of Pharmaceutical Sciences 17 (2022) 880–891

Available online at www.sciencedirect.com

ScienceDirect

journal homepage: www.elsevier.com/locate/AJPS

Original Research Paper

Dynamic crosslinked polymeric nano-prodrugs for highly selective synergistic chemotherapy

Shi Wang[a,1], *Yining Song*[b,1], *Jingge Ma*[a], *Xinyang Chen*[a], *Yuanhui Guan*[a], *Hui Peng*[a], *Guoqing Yan*[a,*], *Rupei Tang*[a,*]

[a] *Engineering Research Center for Biomedical Materials, Anhui Key Laboratory of Modern Biomanufacturing, School of Life Sciences, Anhui University, Hefei 230601, China*

[b] *Anhui Engineering Technology Research Center of Biochemical Pharmaceutical, Bengbu Medical College, Bengbu 233030, China*

ARTICLE INFO

Article history:
Received 28 May 2022
Revised 12 September 2022
Accepted 27 September 2022
Available online 29 October 2022

Keywords:
Nano-prodrugs
Precise structure
Size transition
Amino protonation
Synergistic chemotherapy

ABSTRACT

To achieve highly selective synergistic chemotherapy attractive for clinical translation, the precise polymeric nano-prodrugs (PPD-NPs) were successfully constructed via the facile crosslinking reaction between pH-sensitive poly(ortho ester)s and reduction-sensitive small molecule synergistic prodrug (Pt(IV)-1). PPD-NPs endowed the defined structure and high drug loading of cisplatin and demethylcantharidin (DMC). Moreover, PPD-NPs exhibited steady long-term storage and circulation via the crosslinked structure, suitable negative potentials and low critical micelle concentration (CMC), improved selective tumour accumulation and cellular internalization via dynamic size transition and surficial amino protonation at tumoural extracellular pH, promoted efficient disintegration and drug release at tumoural intracellular pH/glutathione, and enhanced cytotoxicity via the synergistic effect between cisplatin and DMC with the feed ratio of 1:2, achieving significant tumour suppression while decreasing the side effects. Thus, the dynamic crosslinked polymeric nano-prodrugs exhibit tremendous potential for clinically targeted synergistic cancer therapy.

1. Introduction

A few polymeric nanotherapeutics, including Abraxane®, DaunoXome®, and Doxil/Caelyx®, have been clinically used for cancer treatment owing to their multiple nanoscale advantages such as improved pharmacokinetics and tumour accumulation [1]. Unfortunately, they fail to improve the survival of clinical patients significantly due to their limitations, such as poor tumour specificity and imprecise regulation over the pharmaceutical components, carrier architectures, drug release, as well as process stability in drug loading [2–5]. Furthermore, limited progress has been

* Corresponding authors.
E-mail addresses: 17017@ahu.edu.cn (G.Q. Yan), tangrp99@iccas.ac.cn (R.P. Tang).
[1] These authors contributed equally to this work.
Peer review under responsibility of Shenyang Pharmaceutical University.

https://doi.org/10.1016/j.ajps.2022.09.004

made in addressing the issues for clinical transformation, despite the emergence of numerous nanomedicines over the past few decades [6]. Therefore, a precise nanomedicine with improved potency must be developed to significantly promote the chemotherapeutic effect attractive for clinical transformation.

Stimuli-response polymeric nano-prodrugs have recently attracted considerable attention, because they maintain the nanoscale advantages and endow several characteristics such as defined structure, extraordinary drug loading capacity, stable circulation, and targeted drug release at the tumour site [7,8]. Nevertheless, most of them only respond to the microenvironment inside the tumour cells for controlled drug release, but cannot simultaneously respond to tumoural extracellular milieu for triggering physicochemical transformation such as PEGylation and dePEGylation, negative-to-positive charge transitions, dynamic size transition, and disintegration upon arrival at the targeted tumour sites [9,10]. Notably, these extracellular changes in tumours could significantly facilitate drug accumulation via facilitating tumour penetration, retention, and cellular uptake [11–13]. Thus, it is necessary to establish a precise polymeric nano-prodrug to stepwise identify differences in the microenvironments outside and inside the tumour cells for significantly enhanced tumour accumulation and programmed drug release. Although conceptually impressive and practically efficient, the tumoural extracellular and intracellular stimuli-responsive nano-prodrugs such as clustered nanoparticles and cluster-bomb-like nanoassembly have complex composition and preparation technology [14,15], which increase the difficulty of clinical translation. Thereby, it is very promising to develop such a sophisticated nano-prodrug using simple functional components and synthetic process.

Tumoural acidity grading amongst blood vessels (pH∼7.4), extracellular matrix (pH ∼6.5–7.0), endosomes (pH∼5.0–6.0) and lysosomes (pH∼4.0–5.0), and higher intracellular levels of glutathione (GSH) can be used to construct the tumoural extra/intracellular pH/reduction dual-sensitive polymeric nano-prodrug [16,17]. Notably, primary amines and ortho ester linkages have been demonstrated to respond to tumoural acidity both outside and inside cells by optimizing the hydrophilic and hydrophobic environments around them [12,18]. Furthermore, the protonation of primary amines on the nanomedicines from blood vessels to tumoural extracellular matrix could be beneficial to both blood circulation and cellular uptake [19–21], and the extracellular hydrolysis of ortho ester linkages in the nanomedicine may trigger a dynamic size change for improved tumour penetration and retention [10]. Moreover, the small molecule prodrug (Pt(IV)−1) consisting of cisplatin and demethylcantharidin (DMC) at a molar ratio of 1:2 exhibits obvious synergistic effect through crosslinking with DNA and inhibiting protein phosphatase 2A (PP2A) respectively, and can further crosslink amino-containing components to construct the tumoural intracellular pH/reduction-triggered polymeric nano-prodrugs with precise structures and extraordinarily high drug loading capacity [22]. Hence, the dynamic crosslinked polymeric nano-prodrugs for highly selective synergistic chemotherapy can be synthesized through the partial crosslinking reaction between Pt(IV)−1 and poly(ortho ester)s with amino groups in the side chains. It could endow storage and circulation stability through the crosslinked structure, suitable potential at neutral conditions, and strong intermolecular interactions such as hydrogen-bond interactions amongst amino, amide, and residual carboxyl groups, electrostatic interactions between the amino groups and Pt(IV)−1 (cisplatin and residual carboxyl groups), and hydrophilic and hydrophobic interactions. Then, it could selectively accumulate at tumour site and promote cellular uptake via enhanced permeability and retention (EPR) effect, residual amino protonation and dynamic size changes triggered by partial degradation of ortho ester linkages in the backbone at tumoural extracellular pH. Finally, it could further achieve synergistic cytotoxicity via intracellular pH/GSH-triggered efficient release of cisplatin and DMC (Scheme 1).

2. Materials and methods

2.1. Materials

Triethylamine (TEA) and N, N-dimethylformamide (DMF) were dried over calcium hydride before use. Cisplatin (99%), N–hydroxy succinimide (NHS, 98%), 2-amino-1,3-propanediol (98%), ethyl trifluoroacetate (99%), 1-(3-dimethylaminopropyl)−3-ethylcarbodiimide hydrochloride (EDC, 98%), succinic anhydride (SA, 99%), demethylcantharidin (DMC, 99.5%), and trinitrobenzene sulfonic acid (TNBSA, 98%) were purchased from Macklin (Shanghai, China). Human and murine hepatic cancer cell lines (HepG2 (passage number: 67) and H22 (passage number: 49)) were acquired from iCell Bioscience Inc (Shanghai, China). Male ICR and Balb/c nude mice (18–22 g) were obtained from Cyagen Biotechnology Co., Ltd (Jiangsu, China), and the care and use of animals followed the guidance of Anhui University Laboratory Animal Ethics and Management Committee (IACUC(AHU)−2022–013).

2.2. Synthesis and characterization of poly(ortho ester amides) with amino groups in the side chains (POEAd-g-NH_2)

POEAd-*g*-NH_2 was synthesized by condensation polymerization between 2,2′-((4,4′-(oxybis(methylene)) bis(1,3-dioxolane-4,2-diyl)) bis(oxy)) diethanamine (OEN) and Bis(2,5-dioxopyrrolidin-1-yl) O,O'-(2-(2,2,2-trifluoroacetamido) propane-1,3-diyl) disuccinate (BOD), and removal of trifluoroacetylation, as previously described [23]. The structure of POEAd-*g*-NH_2 was confirmed by hydrogen nuclear magnetic resonance (^{1}H NMR).

2.3. Synthesis and characterization of small molecule synergistic prodrug (Pt(IV)−1)

Pt(IV)−1 was synthesized using cisplatin as the initiator, which was oxidated by hydrogen peroxide and acylated at both ends by DMC, as described before [22]. Next, its structure was measured by ^{1}H NMR, X-Ray Diffraction (XRD), and Fourier Transform Infrared Spectrum (FTIR).

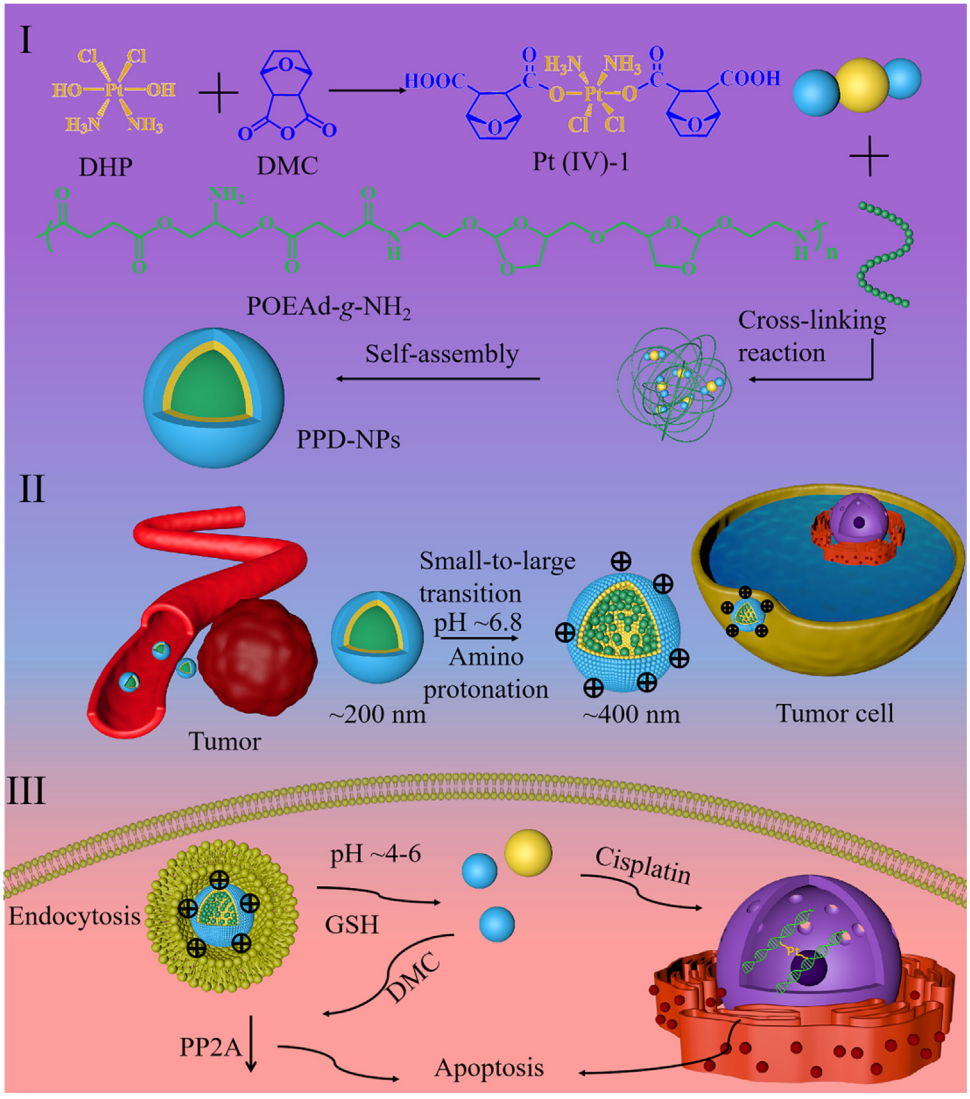

Scheme 1 – Schematic illustration of dynamic crosslinked polymeric nano-prodrugs for highly selective synergistic chemotherapy.

2.4. *Synthesis and characterization of crosslinked polymeric prodrug (PPD)*

A mixture of Pt(IV)−1 (300 mg, 0.45 mmol), NHS (164.9 mg, 1.35 mmol), and EDC (258.8 mg, 1.35 mmol) was dissolved in anhydrous DMF (10 ml) and stirred against light for 12 h under the protection of nitrogen. Next, POEAd-*g*-NH_2 (506.7 mg) containing 0.90 mmol primary amine was added into the above mixture and continued to react for an additional three days. Finally, PPD was yielded by dialysis (MWCO 3500 Da) against deionized (DI) water with a trace mount of TEA and subsequent lyophilization. The structure of PPD was confirmed via ^{1}H NMR, inductively coupled plasma mass spectrometry (ICP-MS), and TNBSA assay [24]. The grafting degree (GD) and crosslinking degree (CD) were respectively calculated according to the following formulas:

$$\text{GD (\%)} = \frac{\textit{content of reacted carboxyl at one end in Pt(IV)} - 1}{\textit{total amino content in POEAd} - g - \text{NH2}} \times 100\%$$

$$\text{CD (\%)} = \frac{\textit{content of reacted carboxyl at both ends in Pt(IV)} - 1}{\textit{total amino content in POEAd} - g - \textit{NH2}} \times 100\%$$

2.5. *Preparation and measurement of PPD-NPs and FITC-labelled PPD-NPs (FITC-PPD-NPs)*

Polymeric nano-prodrugs were prepared using the solvent exchange method [25]. First, amphipathic crosslinked PPD (50 mg) was dissolved in DMSO (0.5 ml) and dropwise added into the slowly stirred DI water (5 ml). Next, the mixture was transferred into dialysis bags (MWCO 3500 Da) and dialyzed against DI water for 24 h, which was replaced every hour. Finally, the dialysate was lyophilized to obtain PPD-NPs, whose CMC was measured using a spectrofluorophotometer with the fluorescence probe, Nile Red, according to the previous literature [25]. Later, the particle sizes, zeta potentials, and morphology of the NPs were measured by dynamic light scattering (DLS) and transmission electron microscopy (TEM). DLS was also used to measure their

stability in PBS (pH 7.4) and SDS (20 mg/ml) for seven days. FITC-PPD-NPs were prepared via the amide reaction between PPD-NPs and a trace amount of FITC in PBS (pH 9.0) and dialysis against DI water. The drug loading efficiency (DLE) of cisplatin and DMC was calculated according to the following formulas:

$$\text{DLC (\%)} = \frac{\textit{the amount of drug in DDP} - \textit{NPs}}{\textit{the amount of DDP} - \textit{NPs}} \times 100\%$$

2.6. Determination of hydrolysis rate of ortho ester linkages in PPD-NPs

PPD-NPs (15 mg) were dispersed in various PBS (pH 7.4, 6.8 and 5.0) and lyophilized at predetermined time intervals. Each sample was then dissolved in d_6-DMSO for ^{1}H NMR analysis. The hydrolysis rate of the ortho ester linkages was determined using the integral area ratio between the peaks at 8.23 and 8.26 ppm and those at 5.79, 8.23, and 8.26 ppm in ^{1}H NMR.

2.7. Detection of changes in particle sizes, zeta potentials, and morphologies

PPD-NPs (10 mg) were separately dispersed in various solutions (pH 7.4, 6.8 and 5.0/GSH (10 mmol/l)) at the final concentration of 1 mg/ml. Each sample was then detected by DLS and/or TEM at predetermined time intervals.

2.8. In vitro drug release from PPD-NPs

PPD-NPs (1 ml) containing 1 mg of cisplatin were separately dialyzed (MWCO 3500 Da) against 10 ml of various solutions (pH 7.4, 6.8 and 5.0/GSH) under mechanical shaking at 37 °C. The dialysates were replaced with fresh PBS at predetermined time points (0, 1, 2, 4, 8, 12 and 24 h). Then, Pt content in each sample was measured by ICP-MS after the treatment with hydrogen peroxide and nitric acid [22], and the DMC content was detected using HPLC [26].

2.9. In vitro cellular uptake

The experiment was performed as described before [12]. In brief, two types of hepatic cancer cells were inoculated in 6-well plates at the density of 1×10^5 cells/well with or without coverslips and cultured for 1 d. FITC-PPD-NPs (8 mg/ml) were added into the 6-well plates and co-incubated with tumour cells for 4 h, after replacement of the medium with fresh one with pH 7.4 and 6.8, consecutively. Next, the tumour cells washed using PBS, immobilized using paraformaldehyde (4%), and dyed using Hoechst33324 were qualitatively determined using a laser scanning confocal microscope (CLSM), and those treated with washing, enzyme digestion, and centrifugation were quantitatively determined using a flow cytometry microscope (FCM).

Two types of hepatic cancer cells were seeded in 6-well plates at the density of 1×10^5 cells/well and continued to culture in a cell incubator at 37 °C. After 24 h, various formulations with the cisplatin concentration of 16 μg/ml were co-cultured with the cells for 4 h. Then, the cells were treated by wash twice, lysis for 30 min at 4 °C, suspension using cell scraper, and centrifugation at 1.2×10^4 rpm. Finally, the cisplatin content in extract liquor was calculated and analysed using ICP-MS.

2.10. In vitro cytotoxicity assay

The experiment was performed as described before [22]. In brief, two types of hepatic cancer cells were seeded in 96-well plates (1×10^5 cells/well) and cultured for one day. Various formulations (Cisplatin/DMC (1:2), Pt(IV)−1, and PPD-NPs) with the same cisplatin content gradient (0.5 to 16 μg/ml) were co-cultured with tumour cells for another two days, after the medium was replaced with fresh medium with pH 7.4 and 6.8 consecutively. Then, the tumour cells per well were sequentially inoculated with MTT for 4 h, washed three times with PBS, immersed in DMSO (150 μl), and measured at UV–vis absorption wavelength of 570 nm using a microplate reader. POEAd-*g*-NH_2 (0.5, 1, 2, 4, 8, 16, 32, 64 and 128 μg/ml) was also applied to co-incubate with HepG2 to determine its cytotoxicity.

2.11. Determination of apoptosis, Pt-DNA adduct content and PP2A activity

The experiment was performed as described before [12]. In brief, two types of hepatic cancer cells were seeded in 6-well plates (1×10^5 cells/well) and proliferated for one day. Various formulations (Cisplatin/DMC (1:2), Pt(IV)−1, and PPD-NPs) with the same cisplatin content of 16 μg/ml were co-cultured with tumour cells for two days. After being washed three times with PBS, the apoptosis, Pt-DNA adduct content, and PP2A activity of the tumour cells were determined using the Annexin V-FITC/PI cell death detection kit, plasmid extraction kit, and Ser/Thr-phosphatase assay kit based on the respective manufacturers' protocols.

2.12. Pharmacokinetics and in vivo biodistribution

The experiment was performed as described before [12]. In brief, drug content in blood, normal tissues (heart, liver, spleen, lung, and kidney) and tumour tissues were evaluated by intravenous administration of various formulations (Cisplatin/DMC (1:2), Pt(IV)−1, and PPD-NPs) to H22 tumour-bearing ICR mice at a cisplatin concentration of 6 mg/kg. The blood, normal tissues and tumours were surgically obtained and weighed at preset time points (2 h, 4 h, 8 h, 12 h, 24 h and 48 h). Pt content of samples was measured by ICP-MS after nitrolysis.

2.13. In vivo antitumour ability

The experiment was performed as described before [12]. In brief, *in vivo* tumour suppression assay was performed using the H22 tumour-bearing ICR mice and HepG2 tumour-bearing nude mice, which were intravenously injected with various formulations (Cisplatin/DMC (1:2), Pt(IV)−1, and PPD-NPs) with the cisplatin content of 6 mg/kg, once the initial tumour volume reached about 150 mm^3. The respective body weights and tumour sizes were monitored each day. The normal organs (heart, liver, spleen, lung, and kidney) and

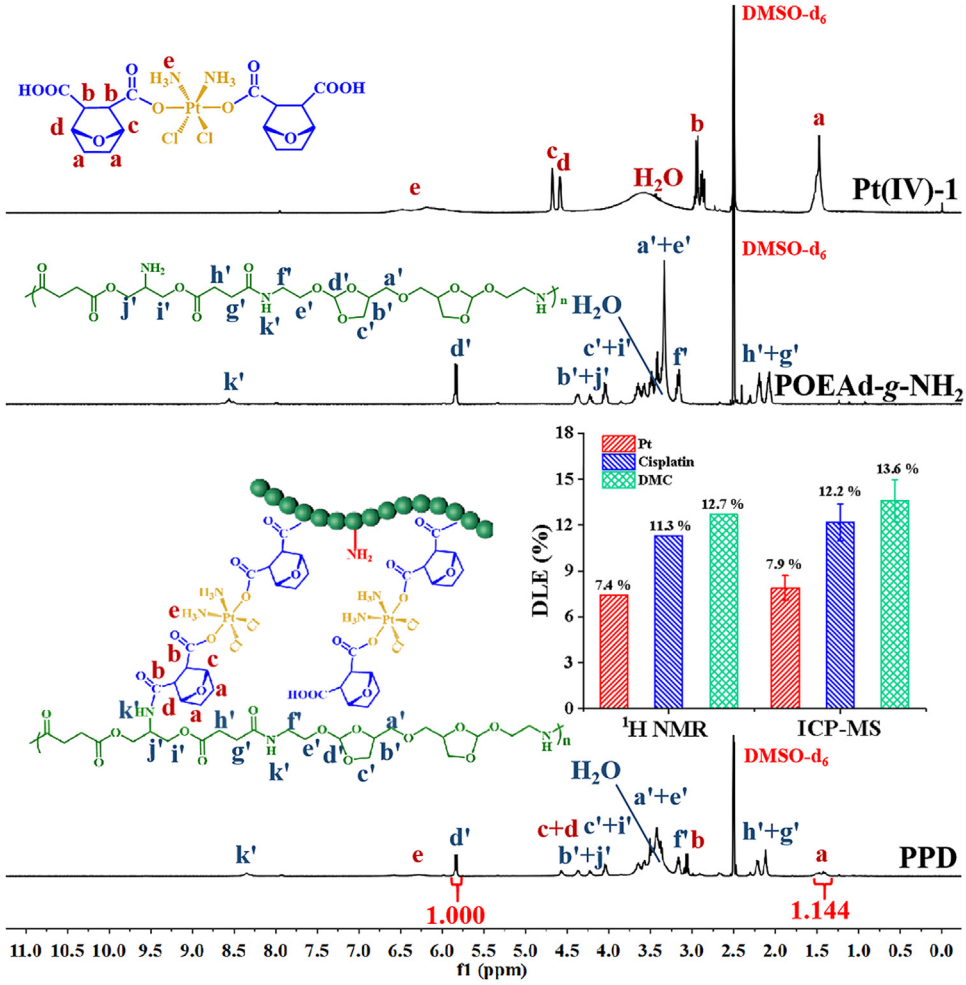

Fig. 1 – ^{1}H NMR spectra of Pt(IV)–1, POEAd-*g*-NH_2 and PPD, and DLE of dual drugs in PPD determined by ^{1}H NMR and ICP-MS.

tumours were surgically obtained to measure the weight and dyed with H&E and TUNEL after the experiment ended. Moreover, the tumours were also photographed, and treated to detect the content of Pt-DNA adduct and expression of PP2A.

2.14. *Statistical analysis*

Results were displayed as mean ± SD. P values were calculated via one-way ANOVA (*$P < 0.05$, **$P < 0.01$, and ***$P < 0.001$). All statistical analyses were conducted using SPSS.

3. Results and discussion

3.1. *Preparation and characterization of crosslinked PPD and PPD-NPs*

As shown in Scheme S1 (Supplementary Data) and Figs. 1, S1 and S2, POEAd-*g*-NH_2 and Pt(IV)−1 were first synthesized as described previously [22,23], and their structures were confirmed using ^{1}H NMR, XRD and FT-IR. Then, the crosslinked PPD was easily synthesized via the amide reaction between POEAd-*g*-NH_2 and Pt(IV)−1, and the feed ratio was precisely tuned to reach about 50% of amino consumption to balance the conflict between the high drug loading and large electronegativity for the blood circulation stability and the cellular internalization by further self-assembly into nano-prodrugs [17,27,28], due to the opposite electrical properties between amino groups in POEAd-*g*-NH_2 and cisplatin in Pt(IV)−1. The structure of the crosslinked PPD was determined by FTIR, ^{1}H NMR, TNBSA, and ICP-MS. As shown in Fig. S2, the decrease of $\delta_{HO-O=}$ at 920 cm^{-1} in FTIR of PPD-NPs suggested the sucessful reaction, compared to that of Pt(IV)−1. As displayed in Fig. 1, the hydrogen protons in PPD had corresponding characteristic peaks in ^{1}H NMR. Moreover, the molar ratio between Pt(IV)−1 and constitutional units of POEAD-*g*-NH_2 was confirmed as 28% using the integral area ratio between the peak at 1.45 ppm (-CH–CH_2–CH_2-, a) and that at 5.80 ppm (-CH–O_3-, d'). Thus, the drug loading of cisplatin and DMC was further calculated as 11.3% and 12.7%, respectively, similar to the results of ICP-MS. In addition, the crosslinking degree at both ends and grafting degree at one end in PPD were further confirmed as 46.8% and 5.2% respectively, by combining with the amino substitution degree (52%) determined by TNBSA [24]. Therefore, the PPD exhibited a precise structure and high drug loading as well as the potential to construct stable nano-prodrugs through strong intermolecular interactions

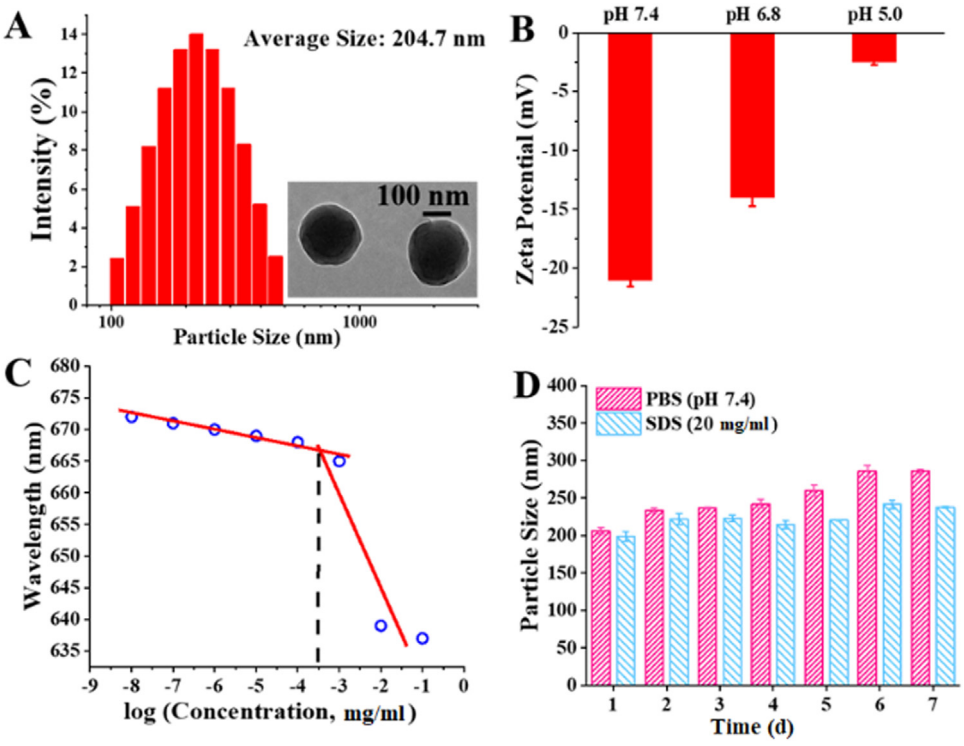

Fig. 2 – Particle sizes (A), zeta potentials (B), CMC (C), and stability in PBS and SDS (D) of PPD-NPs, respectively; Data represent mean ± SD ($n = 3$).

such as hydrogen-bond interactions amongst amino, amide, and residual carboxyl groups, electrostatic interactions between the amino groups and Pt(IV)−1 (cisplatin and residual carboxyl groups), and hydrophilic and hydrophobic interactions.

The amphiphilic crosslinked PPD could easily self-assemble into nano-prodrugs (PPD-NPs) using the solvent exchange method, whose particle sizes, zeta potentials, CMC, and stability in PBS and SDS were confirmed by DLS and/or TEM, as shown in Fig. 2. The suitable zeta potentials (−23.7 mV) were attributed to the balance amongst the components with a positive or negative potential, such as cisplatin, carboxyl groups, and residual amino groups. The lower CMC (5.0×10^{-4} mg/ml) was ascribed to the crosslinked structure and strong intermolecular interactions. Moreover, PPD-NPs could retain similar particle sizes for seven days in PBS and SDS, suggesting their long-term storage and circulation stability owing to the crosslinked polymeric structure, suitable negative zeta potentials, and lower CMC [20,29,30].

3.2. *Tumoural extracellular pH sensitivity and intracellular pH/GSH sensitivity*

To investigate the partial degradation of poly(ortho ester)s and the protonation of the amino groups under tumoural extracellular mildly acidic microenvironment, PPD-NPs were dispersed in different fluids (pH 7.4 and 6.8) and lyophilized for ^{1}H NMR analysis or directly determined by DLS at predetermined time points. As shown in Figs. S3and S4, the ortho ester linkages remained unchanged at pH 7.4, but partially degraded at pH 6.8 in 24 h. This indicated that PPD-NPs retained the chemical stability in blood vessels and pH response in the tumoural extracellular milieu, further triggering the dynamic size transition for enhanced tumour accumulation [10,20]. As displayed in Fig. 2B, the zeta potentials transformed from −23.7 mV at pH 7.4 to −13.1 mV at pH 6.8. The result implied that the residual amino groups (48%) were protonated to decrease the surficial negative potentials for improved cellular uptake [11,20].

PPD-NPs were also suspended in PBS (pH 5.0) for determining the intracellular pH sensitivity. As seen in Fig. 2B, the zeta potentials got larger and changed to be −2.5 mV at pH 5.0 through further amino protonation. As shown in Figs. S3 and S4, the ortho ester linkages were fully degraded in 24 h, suggesting the rapid disintegration of the skeleton in PPD-NPs. In addition, the amide bonds between DMC and amino groups were also easily hydrolysed via intracellular acidolysis and anchimeric assistance, once the tetravalent cisplatin was reduced by the high intracellular GSH [22]. The efficient hydrolysis of poly (ortho ester)s and reduction of tetravalent cisplatin following the degradation of amide bond may result in rapid intracellular disintegration of PPD-NPs and efficient drug release [22,23,31].

3.3. *Size transition triggered by pH/GSH sensitivity*

To evaluate the effect of pH/GSH sensitivity on size transition, PPD-NPs were separately dispersed in various environmental

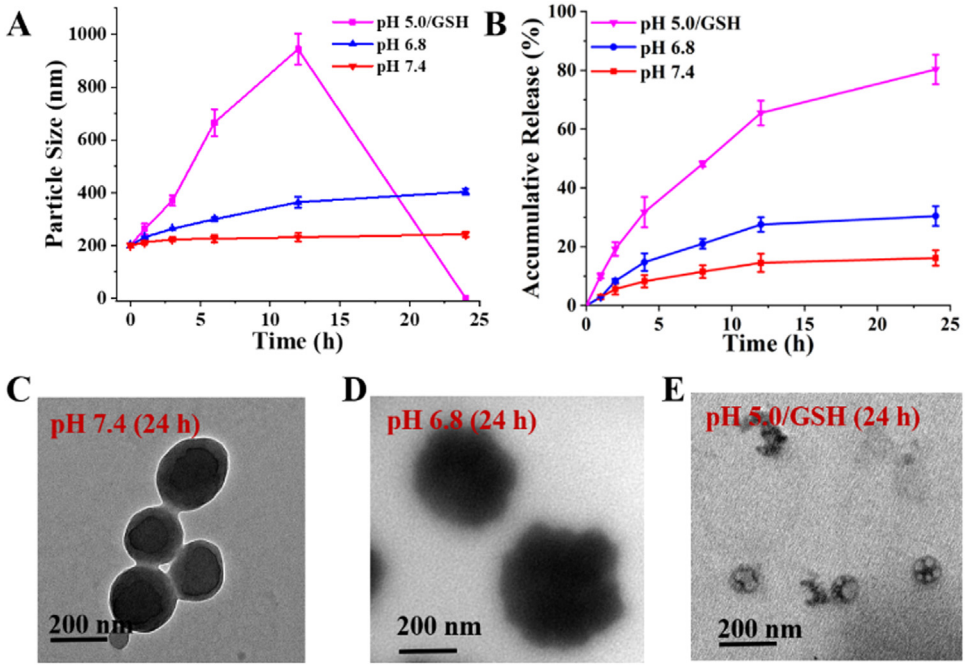

Fig. 3 – Size transition (A, C-E) and accumulative drug release (B) of PPD-NPs under different conditions following time course; Data represent mean ± SD ($n = 5$).

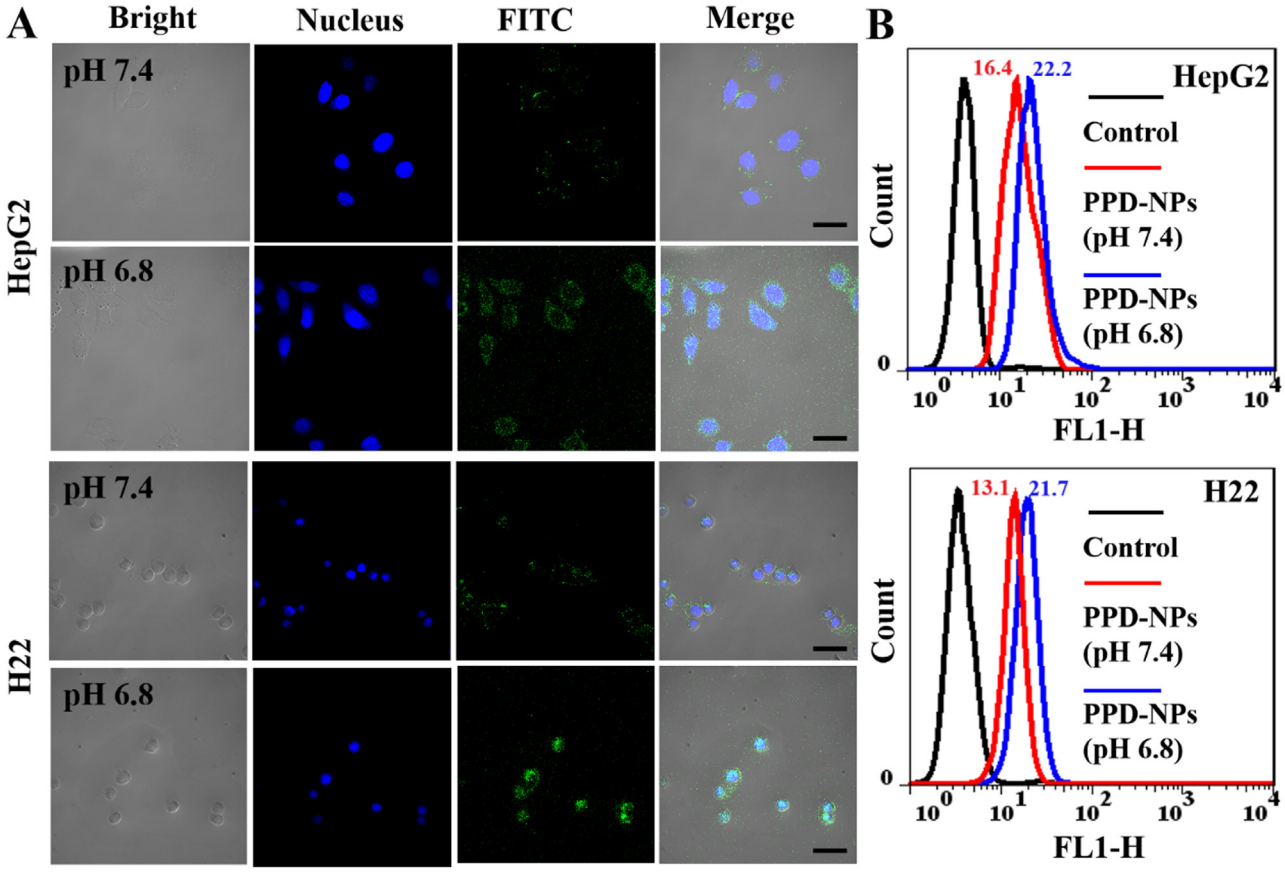

Fig. 4 – Cellular uptake of FITC-PPD-NPs measured by CLSM (A) and FCM (B) respectively; Scale bar = 10 μm.

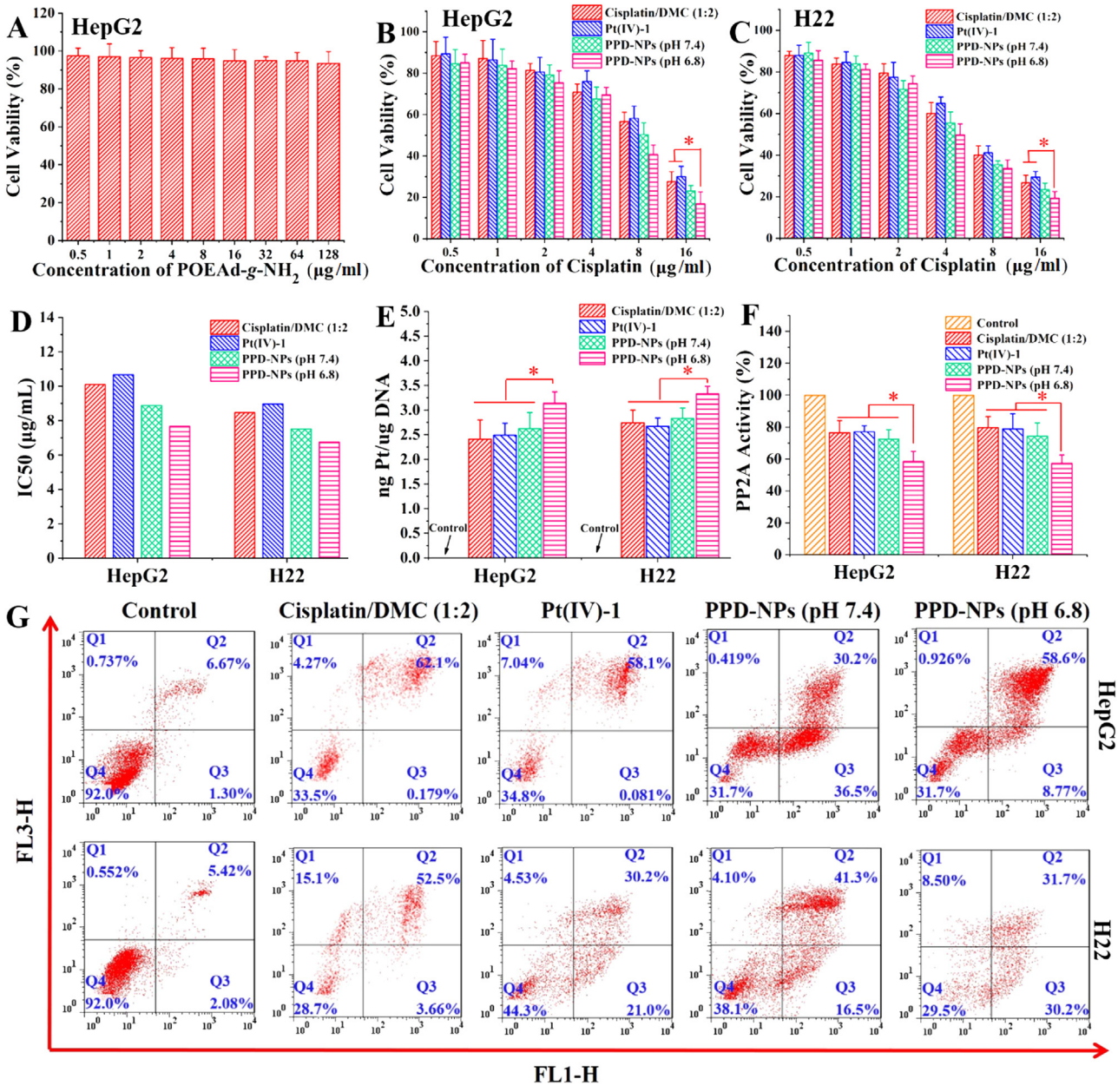

Fig. 5 – *In vitro* cytotoxicity (A-C), IC50 values (D), content of Pt-DNA adducts (E), PP2A activity (F), and apoptosis (G) of various formulations against HepG2 and H22 for 48 h respectively; Data represent mean ± SD ($n = 5$).

simulation fluids (pH 7.4, 6.8 and 5.0/GSH). As shown in Fig. 3A and 3C-3E, the particle sizes stayed the same for 24 h at pH 7.4 based on their stable physicochemical properties under neutral conditions. However, the particle sizes exhibited different trends of change at pH 6.8 and pH 5.0/GSH. The particle sizes gradually increased from 200 to 400 nm in 24 h at pH 6.8 following the partial hydrolysis of poly(ortho ester)s, but sharply increased from 200 to 950 nm in 12 h, and rapidly disintegrated in another 12 h at pH 5.0/GSH owing to the complete hydrolysis of ortho esters and amido bonds, and reduction of tetravalent cisplatin. The tumoural extracellular small-to-large size transition was beneficial to drug retention and accumulation [12], and intracellular rapid disintegration facilitated efficient drug release [10].

3.4. *Drug release based on size transition*

To evaluate the influence of size transition on drug release, PPD-NPs were also dialyzed against various environmental simulation fluids, and Pt contents of the dialysates were determined by ICP-MS. As seen in Fig. 3B, less than 10% of cisplatin was released from PPD-NPs at pH 7.4 in 24 h, owing to constant particle sizes based on stable physicochemical properties under neutral conditions. PPD-NPs released about 20% of cisplatin at pH 6.8 in 24 h owing to the loose structure triggered by partial degradation of poly(ortho ester)s. In fact, cisplatin existed as the prodrug in dialysates at pH 6.8 and could not be released in the absence of GSH [32]. In contrast, above 80% of cisplatin was released from PPD-NPs in 24 h due to rapid disintegration at pH 5.0/GSH. In

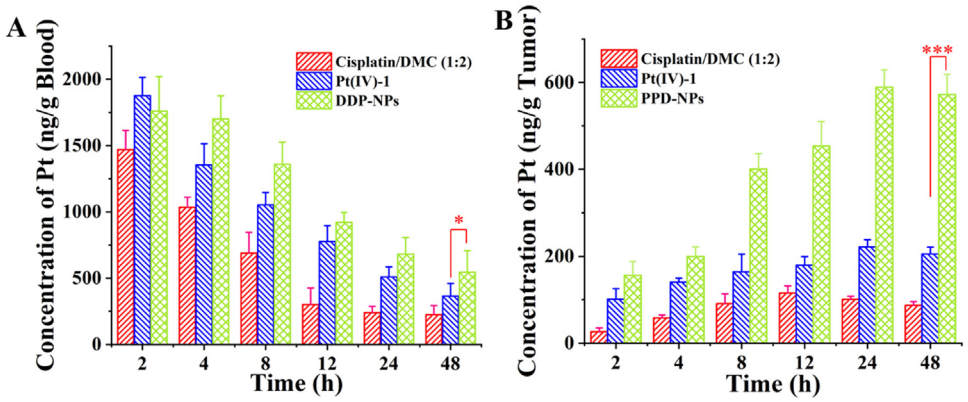

Fig. 6 – Variation tendency of Pt biodistribution in blood (A) and tumour tissue (B) on H22 tumour-bearing ICR mice following time course after treatment of various formulations; Data represent mean ± SD ($n = 3$).

addition, as shown in Fig. S5, DMC exhibited similar release trends with cisplatin because of their bonding together, and effective degradation at tumoural intracellular pH/GSH [33]. Furthermore, the intracellular efficient drug release could promote cytotoxicity.

3.5. *Cellular uptake, cytotoxicity, and apoptosis analysis*

We analysed the cellular uptake, cytotoxicity, and apoptosis to investigate the impact of extracellular amino protonation, dynamic size transition, high-efficiency intracellular drug release as well as synergy of cisplatin and DMC of PPD-NPs upon pharmacological activity by co-culturing PPD-NPs with HepG2 and H22. POEAd-*g*-NH_2 was also applied to co-incubate with HepG2 as control. As seen in Fig. 4, PPD-NPs were effectively ingested by both types of tumour cells as determined by qualitative and quantitative analyses. Moreover, as shown in Fig. S6, PPD-NPs exhibited higher cellular uptake than other formulations, and Pt intake at pH 6.8 was 1.5 times higher than that at pH 7.4 through amino protonation of PPD-NPs [18,19]. The effective cellular uptake was further beneficial to tumoural cytotoxicity. As shown in Fig. 5A-5F, POEAd-*g*-NH_2 as control could not inhibit the cell proliferation, but all formulations including cisplatin and DMC exhibited significant cytotoxicity through cross-binding with DNA and inhibition of PP2A activity [34]. The result suggested that the cytotoxicity was yielded by the synergistic effect of cisplatin and DMC with the feed ratio of 1:2 [22]. Moreover, PPD-NPs best inhibited the tumour cell growth at pH 6.8 via the improved cellular uptake, efficient drug release, and synergistic cytotoxicity between cisplatin and DMC. In addition, to further demonstrate whether cytotoxicity was induced by apoptosis, two types of tumour cells were sequentially co-incubated with various formulations for 48 h, dyed with Annexin V-FITC/PI, and determined by FCM. As shown in Fig. 5G, the apoptosis rates of HepG2 were 62.3%, 58.2%, 66.7% and 67.4%, and the apoptosis rates of H22 were 56.2%, 51.2%, 57.8% and 61.9% caused by cisplatin/DMC (1:2), Pt(IV)−1, PPD-NPs (pH 7.4) and PPD-NPs (pH 6.8), respectively. This implied that cytotoxicity was mainly induced by apoptosis [35], and the apoptosis trends were similar in the consequences of cytotoxicity.

3.6. *Pharmacokinetics and in vivo biodistribution*

To explore the effect of lower CMC, suitable particle sizes and zeta potentials, dynamic size transition and amino protonation on pharmacokinetics and biodistribution of PPD-NPs, various formulations were injected intravenously into the H22 tumour-bearing mice, and blood, tumours and normal tissues were surgically obtained at desired time points. As shown in Fig. 6A, the cisplatin content quickly decreased from 1468.94 to 225.05 ng/g in 48 h for the cisplatin/DMC (1:2) group, suggesting its easy clearance in the blood vessel [36]. Pt(IV)−1 as a small molecular prodrug showed higher cisplatin content ranging from 1877.37 to 365.43 ng/g. PPD-NPs achieved the highest blood drug concentration ranging from 1759.34 to 545.19 ng/g. Furthermore, as shown in Table S1, PPD-NPs displayed the longer half-life period ($T_{1/2}$), and larger area under the concentration-time curve (AUC), maximum blood concentration (C_{max}) and mean residence time (MRT) than other groups, owing to the suitable particle sizes and potentials, stable physicochemical properties, and lower CMC. As seen in Fig. 6B, cisplatin content in the tumour tissues first increased and then decreased, but remained lower than 100 ng/g for the cisplatin/DMC (1:2) group due to the lower blood drug concentration and weaker tumour retention. Pt(IV)−1 showed higher cisplatin content than cisplatin/DMC (1:2), but only increased from 101.40 to 205.34 ng/g. Notably, PPD-NPs exhibited significantly higher drug content ranging from 180.21 to 593.67 ng/g in tumour tissues than other formulations via the higher blood drug concentration, dynamic size transition for the enhanced tumour retention, and amino protonation for the improved cellular uptake [10,18,20]. In addition, the highly selective tumour accumulation was beneficial to an efficient tumour suppression. Moreover, as displayed in Fig. S7, PPD-NPs exhibited the lower drug concentration in normal tissues (heart, spleen, lung, and kidney) compared to other formulations, suggesting their less side effects.

3.7. *In vivo antitumour activity*

H22 tumour-bearing mice were used to explore the influence of the enhanced tumour accumulation and cellular uptake,

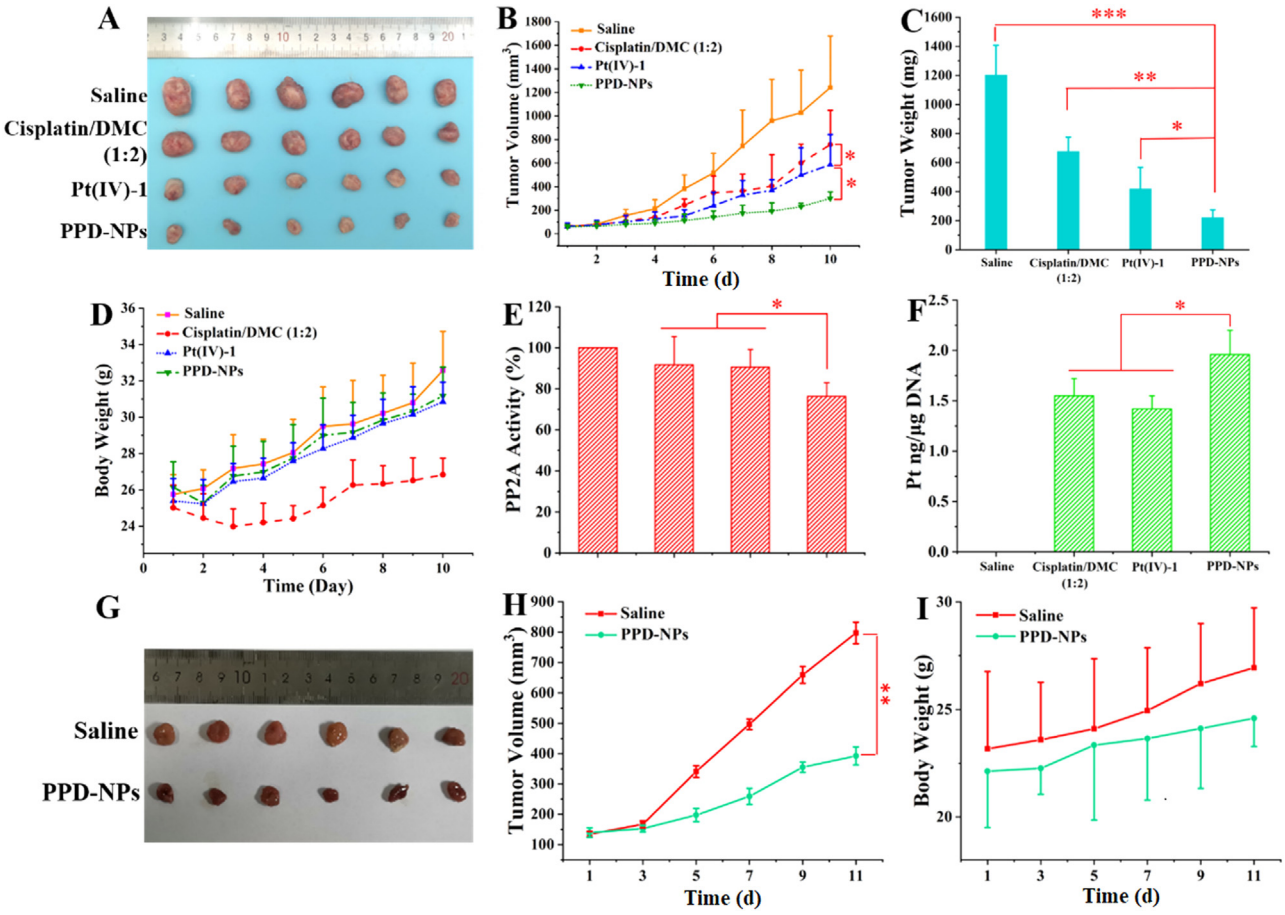

Fig. 7 – Tumour photo (A), tumour growth curve (B), tumour weight (C), body weight change (D), and tumoural PP2A activity (E) and Pt-DNA adducts (F) on ICR mice bearing subcutaneous H22 tumour model; Tumour photo (G), tumour growth curve (H) and body weight change (I) on nude mice bearing subcutaneous HepG2 tumour mode; Data represent mean ± SD ($n = 6$).

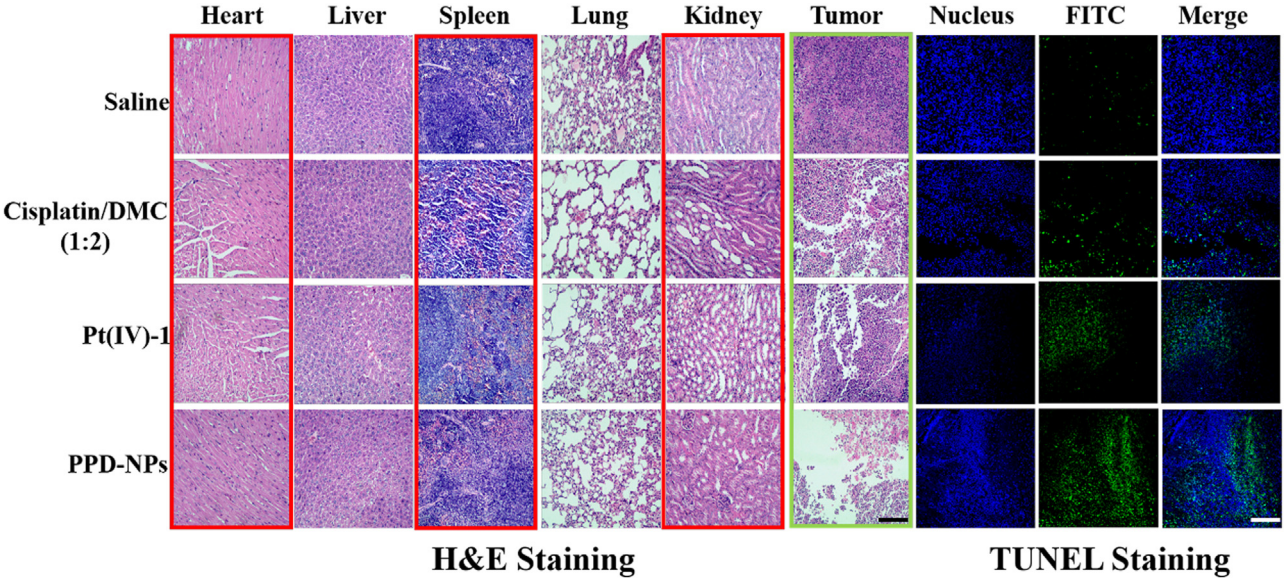

Fig. 8 – Histological analysis by H&E staining and TUNEL staining; Scale bar = 100 μm.

high-efficiency intracellular drug release, and synergy of cisplatin and DMC on tumour inhibition. As shown in Fig. 7A-7C, various formulations containing cisplatin and DMC exhibited significant tumour inhibition compared with saline. However, cisplatin/DMC (1:2) resulted in weight loss and destruction of integrity of heart, spleen, and kidney (Figs. 7D and 8), indicating its serious side effects [37,38]. Pt(IV)−1 also gave rise to systemic toxicity and destroyed the integrity of heart and kidney to some degree (Fig. 8), although it showed a stronger ability to inhibit tumour growth than cisplatin/DMC (1:2) through higher tumour accumulation. Notably, PPD-NPs achieved the best tumour inhibition with no apparent systemic toxicity via the highly selective tumour accumulation, enhanced cellular uptake, efficient drug release and synergistic cytotoxicity. Moreover, the antitumour mechanism was evaluated through detecting the apoptosis, expression of PP2A and Pt-DNA adduct at tumour tissues. As seen in Fig. 7E and 7F, PPD-NPs displayed the stronger ability to inhibit the expression of PP2A and cross-bind to DNA at tumour tissues via the role of DMC and cisplatin respectively, thus achieving the improved apoptosis in comparison with other formulations (Fig. 8). Furthermore, as shown in Fig. 7G-7I, HepG2 tumour-bearing nude mice were also established to investigate the antitumour activity of crosslinked polymeric nano-prodrugs. The result suggested that DDP-NPs could also significantly inhibit the tumour growth compared to the control.

4. Conclusion

In summary, the crosslinked PPD was synthesized via the amide reaction between POEAd-*g*-NH_2 and Pt(IV)−1, and then self-assembled into nano-prodrugs in a neutral pH condition. The nano-prodrugs showed high drug loading, lower CMC, and long-term stability in PBS and SDS. Moreover, the nano-prodrugs exhibited small-to-large particle size transition and surficial amino protonation at pH 6.8, and effective disintegration and drug release at pH 5.0/GSH. These characteristics enabled nano-prodrugs to maintain high blood drug concentration and enhance tumour accumulation, cellular uptake, and synergistic cytotoxicity, thereby achieving significant tumour suppression while decreasing their side effects on normal tissues. By further optimization, the dynamic crosslinked polymeric nano-prodrugs could potentially be applied for highly selective cancer therapy for clinical applications.

Conflicts of interest

The authors report no conflicts of interest. The authors alone are responsible for the content and writing of this article.

Acknowledgments

This work was supported by the Anhui Engineering Technology Research center of Biochemical Pharmaceutical (Bengbu Medical College), the National Natural Science Foundation of China (No. 51803001), the Research Foundation of Education Department of Anhui Province of China (No. KJ2018ZD003, KJ2018A0006 and KJ2019A0015), and the Academic and Technology Introduction Project of Anhui University (AU02303203).

Supplementary materials

Supplementary material associated with this article can be found, in the online version, at doi:10.1016/j.ajps.2022.09.004.

REFERENCES

[1] Younis MA, Tawfeek HM, Abdellatif AAH, Abdel-Aleem JA, Harashima H. Clinical translation of nanomedicines: challenges, opportunities, and keys. Adv Drug Deliv Rev 2022;181:114083.
[2] Zheng X, Xie J, Zhang X, Sun W, Zhao H, Li Y, et al. An overview of polymeric nanomicelles in clinical trials and on the market. Chin Chem Lett 2021;32(1):243–57.
[3] Li L, Zuo S, Dong F, Liu T, Gao Y, Yang Y, et al. Small changes in the length of diselenide bond-containing linkages exert great influences on the antitumor activity of docetaxel homodimeric prodrug nanoassemblies. Asian J Pharm Sci 2021;16(3):337–49.
[4] Wang Y, Luo C, Zhou S, Wang X, Zhang X, Li S, et al. Investigating the crucial roles of aliphatic tails in disulfide bond-linked docetaxel prodrug nanoassemblies. Asian J Pharm Sci 2021;16(5):643–52.
[5] Yang L, Xu J, Xie Z, Song F, Wang X, Tang R. Carrier-free prodrug nanoparticles based on dasatinib and cisplatin for efficient antitumor *in vivo*. Asian J Pharm Sci 2021;16(6):762–71.
[6] Gan WW, Chan LW, Li W, Wong TW. Critical clinical gaps in cancer precision nanomedicine development. J Control Release 2022;345:811–8.
[7] Nguyen A, Böttger R, Li SD. Recent trends in bioresponsive linker technologies of prodrug-based self-assembling nanomaterials. Biomaterials 2021;275:120955.
[8] Dong X, Brahma RK, Fang C, Yao SQ. Stimulus-responsive self-assembled prodrugs in cancer therapy. Chem Sci 2022;13:4239.
[9] Zhang Y, Cao J, Yuan Z. Strategies and challenges to improve the performance of tumour-associated active targeting. J Mater Chem B 2020;8(18):3959–71.
[10] Hu J, Yuan X, Wang F, Gao H, Liu X, Zhang W. The progress and perspective of strategies to improve tumour penetration of nanomedicines. Chin Chem Lett 2020;32(4):1341–7.
[11] Chang D, Ma Y, Xu X, Xie J, Ju S. Stimuli-responsive polymeric nanoplatforms for cancer therapy. Front Bioeng Biotechnol 2021;9:1–26.
[12] Yang L, Yan G, Wang S, Xu J, Fang Q, Xue Y, et al. Dynamic precise dual-drug-backboned nano-prodrugs for selective chemotherapy. Acta Biomater 2021;129:209–19.
[13] Jia N, Li W, Liu D, Wu S, Song B, Ma J, et al. Tumour microenvironment stimuli-responsive nanoparticles for programmed anticancer drug delivery. Mol Pharmacol 2020;17(5):1516–26.
[14] Sun Q, Sun X, Ma X, Zhou Z, Jin E, Zhang B, et al. Integration of nanoassembly functions for an effective delivery cascade for cancer drugs. Adv Mater 2014;26:7615–21.

[15] Li HJ, Du JZ, Du XJ, Xu CF, Sun CY, Wang HX, et al. Stimuli-responsive clustered nanoparticles for improved tumor penetration and therapeutic efficacy. Proc Natl Acad Sci USA 2016;113:4164.
[16] Gong F, Yang N, Wang X, Zhao Q, Chen Q, Liu Z, et al. Tumour microenvironment-responsive intelligent nanoplatforms for cancer theranostics. Nano Today 2020;32:100851.
[17] Chen M, Liu D, Liu F, Wu Y, Peng X, Song F. Recent advances of redox-responsive nanoplatforms for tumour theranostics. J Control Releas 2021;332:269–84.
[18] Sun Q, Zhu Y, Du J. Recent progress on charge-reversal polymeric nanocarriers for cancer treatments. Biomed Mater 2021;16(4):042010.
[19] Yan Y, Ding H. pH-responsive nanoparticles for cancer immunotherapy: a brief review. Nanomaterials 2020;10(8):1–15.
[20] Zhao Q, Zhang S, Wu F, Li D, Zhang X, Chen W, et al. Rational design of nanogels for overcoming the biological barriers in various administration routes. Angew Chem Int Ed 2021;60(27):14760–78.
[21] Fang Z, Pan S, Gao P, Sheng H, Li L, Shi L, et al. Stimuli-responsive charge-reversal nano drug delivery system: the promising targeted carriers for tumour therapy. Int J Pharmacol 2020;575:118841.
[22] Cong Y, Xiao H, Xiong H, Wang Z, Ding J, Li C, et al. Dual drug backboned shattering polymeric theranostic nanomedicine for synergistic eradication of patient-derived lung cancer. Adv Mater 2018;30(11):1706220.
[23] Yan G, Wang J, Hu L, Wang X, Yang G, Fu S, et al. Stepwise targeted drug delivery to liver cancer cells for enhanced therapeutic efficacy by galactose-grafted, ultra-pH-sensitive micelles. Acta Biomater 2017;51:363–73.
[24] Simoes LS, Martins JT, Pinheiro AC, Vicente AA, Ramos OL. Beta-lactoglobulin micro- and nanostructures as bioactive compounds vehicle: *in vitro* studies. Food Res Int 2020;131:108979.
[25] Bixenmann L, Stickdorn J, Nuhn L. Amphiphilic poly(esteracetal)s as dual pH-and enzyme-responsive micellar immunodrug delivery systems. Polym Chem 2020;11(13):2441–56.
[26] Yan Z, Yang K, Tang X, Bi Y, Ding Y, Deng M, et al. Norcantharidin nanostructured lipid carrier (NCTD-NLC) suppresses the viability of human hepatocellular carcinoma HepG2 cells and accelerates the apoptosis. J Immunol Res 2022;2022:3851604.
[27] Wang J, Ni Q, Wang Y, Zhang Y, He H, Gao D, et al. Nanoscale drug delivery systems for controllable drug behaviors by multi-stage barrier penetration. J Control Release 2021;331:282–95.
[28] Francia V, Montizaan D, Salvati A. Interactions at the cell membrane and pathways of internalization of nano-sized materials for nanomedicine. Beilstein J Nanotech 2020;11:338–53.
[29] Chen J, Garcia ES, Zimmerman SC. Intramolecularly cross-linked polymers: from structure to function with applications as artificial antibodies and artificial enzymes. ACC Chem Res 2020;53(6):1244–56.
[30] Ghezzi M, Pescina S, Padula C, Santi P, Del Favero E, Cantù L, et al. Polymeric micelles in drug delivery: an insight of the techniques for their characterization and assessment in biorelevant conditions. J Control Release 2021;332:312–36.
[31] Scorsin L, Affeldt RF, Oliveira BS, Silveira EV, Ferraz MS, de Souza FPS, et al. Coordination among bond formation/cleavage in a bifunctional-catalyzed fast amide hydrolysis: evidence for an optimized intramolecular N-protonation event. J Org Chem 2020;85(7):4663–71.
[32] Chen KJ, Plaunt AJ, Leifer FG, Kang JY, Cipolla D. Recent advances in prodrug-based nanoparticle therapeutics. Eur J Pharm Biopharm 2021;165:219–43.
[33] Liu C, Li C, Pang C, Li M, Li H, Li P, et al. Supramolecular drug-drug complex vesicles enable sequential drug release for enhanced combination therapy. ACS Appl Mater Interfaces 2020;12(25):27940–50.
[34] Xie P, Wang Y, Wei D, Zhang L, Zhang B, Xiao H, et al. Nanoparticle-based drug delivery systems with platinum drugs for overcoming cancer drug resistance. J Mater Chem B 2021;9(26):5173–94.
[35] Hakkarainen H, Aakko-Saksa P, Sainio M, Ihantola T, Ronkko TJ, Koponen P, et al. Toxicological evaluation of exhaust emissions from light-duty vehicles using different fuel alternatives in sub-freezing conditions. Part Fibre Toxicol 2020;17(1):17.
[36] Zhang X, Liu D, Lv F, Yu B, Shen Y, Cong H. Recent advances in ruthenium and platinum based supramolecular coordination complexes for antitumour therapy. Colloids Surf B 2019;182:110373.
[37] Volarevic V, Djokovic B, Jankovic MG, Harrell CR, Fellabaum C, Djonov V, et al. Molecular mechanisms of cisplatin-induced nephrotoxicity: a balance on the knife edge between renoprotection and tumour toxicity. J Biomed Sci 2019;26(1):25.
[38] Qi L, Luo Q, Zhang Y, Jia F, Zhao Y, Wang F. Advances in toxicological research of the anticancer drug cisplatin. Chem Res Toxicol 2019;32(8):1469–86.